
[View Journal Online](#)
[View Article Online](#)

Catalytic activity of nanosized Au/CeO₂ catalyst towards H₂O₂ decomposition and the role of cationic/metallic ratio in its activity

Ayman Abd El-Moemen *

Chemistry Department, Faculty of Science, Suez Canal University, Ismailia, 41522, Egypt

* Corresponding author at: Chemistry Department, Faculty of Science, Suez Canal University, Ismailia, 41522, Egypt.

Tel: +20.109.9403540 Fax: +20.64.3230416 e-mail: ayman.moemen@science.suez.edu.eg (A.A. El-Moemen).

RESEARCH ARTICLE

ABSTRACT



doi: 10.5155/eurjchem.10.4.317-322.1895

Received: 20 May 2019
 Received in revised form: 12 July 2019
 Accepted: 13 July 2019
 Published online: 31 December 2019
 Printed: 31 December 2019

The catalytic decomposition of H₂O₂ on differently pre-treated Au/CeO₂ catalyst was studied by kinetic measurements at 20-50 °C. The prepared catalyst was subjected to pre-treatment by heating either in oxidative (10% O₂/N₂) or inert (pure N₂) atmosphere at 400 °C. The different oxidation states of gold were determined by X-ray photoelectron spectroscopy measurements. The Au/CeO₂ catalyst exhibited an excellent catalytic activity towards H₂O₂ decomposition. The catalytic activity of oxygen pre-treated sample was about twice higher than that measured for nitrogen pre-treated sample. This finding ran parallel to the amount of Au³⁺ as determined by XPS, indicating the role played by Au³⁺ species as the most active catalyst's constituent. However, one cannot overlook the role of metallic gold in catalyzing the H₂O₂ decomposition showing small activity compared to that of cationic gold. The average crystallites size of metallic gold particles was found to be 7±0.5 nm independent of the pre-treatment conditions. The apparent activation energy of the catalyzed reaction was found to be 46.5 and 47.8 kJ/mol for oxygen and nitrogen pre-treatment, respectively.

KEYWORDS

Au/CeO₂ catalyst
 Catalytic activity
 H₂O₂ decomposition
 Catalyst pre-treatment
 X-ray diffraction (XRD)
 X-ray photoelectron spectroscopy (XPS)

Cite this: *Eur. J. Chem.* 2019, 10(4), 317-322Journal website: www.eurjchem.com

1. Introduction

H₂O₂ decomposition reaction has been extensively studied [1-10]. This is mainly due to the following reasons: (i) H₂O₂ decomposition is a useful model test reaction for studying the catalytic activity of different materials, (ii) H₂O₂ might be an efficient oxygen source, if highly active and selective catalysts are used. (iii) H₂O₂ used as an oxidant (clean oxidizing agent or ideal liquid phase green oxidation processes) in the presence of a good and selective catalyst, for organic synthesis, and water treatment technologies as it emits only H₂O by product with high atom efficiency. Various organic water and soil pollutants can be successfully oxidized and degraded by hydrogen peroxide promoted by iron oxides [11-13].

Recently as a development of fuel cell technology, both water gas shift reaction and CO oxidation reaction are important for the removal of CO from the fuel cell [14,15]. On the other hand, one of the most important problems in Proton Exchange Membrane Fuel Cell (PEMFC) technology, is a production of H₂O₂ electrochemically or chemically during operation at the cathode as a by-product, and therefore may deteriorate materials in the membrane-electrode [14,16]. Using a highly active and selective catalyst in the PEMFC may be working in more than one way simultaneously, decompo-

sition of H₂O₂ and producing of pure oxygen which is sufficient for CO oxidation.

In the last few years, gold catalysts supported on metal oxides have been reported to be highly active for several reactions, including the water gas shift (WGS) reaction [17-20], the low temperature CO oxidation by oxygen [21,22], and H₂O₂ decomposition [3]. The catalytic activity of these catalysts is strongly affected by gold particle size, synthesis method, pre-treatment conditions, oxidation state of gold and the nature of the support material [22,23].

It has been reported that, the H₂O₂-Au/support catalytic system has been proven to be effective in removing low-level hazardous organic compounds including formaldehyde, acetone, and phenol from waste water [24]. It is also found that, the catalytic activity of Au/TiO₂ towards the H₂O₂ decomposition strongly depends on the gold particle size, and also exhibits a high activity for the chemoselective oxidation of cinnamyl alcohol to cinnamaldehyde, based on "liquid-phase green oxidation processes" using an H₂O₂-Au/metal oxide system [3,25].

Catalysts based on cerium oxide (Ceria, CeO₂) are promising for these applications. Ceria is widely used as an oxygen storage component in the automobile three-way catalyst. It gives up oxygen under rich engine operating conditions and accepts oxygen under lean conditions.

Table 1. XPS data of gold, and ceria species measured after different pre-treatments.

Catalyst pre-treatment	Au ⁰ (%)	Au ¹⁺ (%)	Au ³⁺ (%)	Au ⁿ⁺ /Au ⁰	Ce ³⁺ (%)	I _{Au(4f)} /I _{Ce(3d)}
Oxygen	35	45	20	1.86	21	0.08
Nitrogen	54	30	16	0.85	23	0.07

Thus, ceria is good for oxygen-storage capacity (OSC). Luo *et al.* found a direct relationship between the WGS activity and the OSC [26]. Different models have been proposed to explain the unique catalytic activity of the CeO₂ supported Au catalysts towards either CO oxidation or WGS reaction. Nano-sized Au/CeO₂ catalyst consisted of metallic and cationic gold species. The role of these species in its activity towards WGS reaction had been investigated by several authors [27-29]. Fu *et al.* reported that non-metallic (cationic) gold species strongly associated with surface cerium-oxygen groups are the most catalytically active constituent [27] while, Kim and Thompson claimed an opposite trend [28]. However, Karpenko *et al.* have reported that the catalytic activity of Au/CeO₂ catalyst towards WGS reaction depends on the contribution of both metallic and cationic gold species present on the catalyst surface [29]. The aim of the present work is to study the effect of synthesis and characterization of the nano-sized Au/CeO₂ system on its activity using H₂O₂ decomposition, and the role of cationic/metallic gold species on the activity of the prepared catalysts. The extent of both metallic and cationic gold in the prepared catalyst was effectively modified by pre-treatment with oxygen or nitrogen at 400 °C.

2. Experimental

2.1. Materials

The nanosized Au/CeO₂ catalyst was prepared by a deposition-precipitation procedure. CeO₂ support material was pre-calcined in air at 400 °C for 4 h and re-dispersed in water at 60 °C. The gold precursor (HAuCl₄·3H₂O) was added dropwise, while adjusting the pH value at 5-6 by adding Na₂CO₃ solution [29]. The Au metal loading was determined via inductively coupled plasma atomic emission spectroscopy (ICP-AES). All measurements were performed with catalysts of 4.5 wt% Au loading. The obtained sample was subjected to heat in a current of 10% O₂/N₂ or pure N₂ flowing at a rate of 20 mL/min at 400 °C for 30 min.

2.2. Techniques

2.2.1. X-ray diffraction measurements

The X-ray investigations of the obtained pre-treated catalysts were carried out using a Bruker diffractometer (Bruker D8 advance target). The scanning rate was fixed for phase identification at 0.018° in 2θ/min for line broadening profile analysis. The patterns were run with CuKα₁ with secondly monochromator (λ = 0.15405 nm) at 40 kV and 35 mA. The crystallite size of each phase present in different solids was calculated, using the line broadening profile analysis by direct application of the Scherrer's equation.

2.2.2. XPS measurements

The chemical composition of the catalyst surface and the oxidation states of both gold and cerium species were characterized by XPS (PHI 5800 ESCA system), using monochromatized Al-Kα radiation. The survey spectra were measured in the range between 0 and 1400 eV binding energy (BE). Detail spectra of gold (Au(4f)) and ceria (Ce(3d)) were measured in the range of 75-100 eV and 875-925 eV (0.125 eV and 20 ms per step), respectively.

2.2.3. Specific surface area

The specific surface area of the prepared sample was measured by nitrogen adsorption isotherm measured at -196 °C using Porotec Sorptomatic 1990 systems. The specific surface area of the prepared catalyst measured 188 m²/g.

2.2.4. Activity measurements

For kinetic measurements, the decomposition of hydrogen peroxide in aqueous medium was studied. The kinetics of reaction was followed up gasometrically according to the technique described by Deren *et al.* [30], using 0.2 M H₂O₂ solution. The catalytic reaction was monitored by measuring the volume of oxygen liberated at different time intervals.

3. Results and discussion

3.1. XPS investigation of different pre-treated catalyst samples

The chemical composition of the catalyst after the oxygen or nitrogen pre-treatments at 400 °C was characterized via the Au(4f) and Ce(3d) signals. For quantitative evaluation, the XPS spectra of the Au(4f) signals were fitted by three different states with BEs of 84.0, 84.6 and 85.9 eV, respectively [28,31-33]. The first and the last peaks are assigned to Au⁰ and Au³⁺ species [32,34,35], while the peak at 84.6 eV was previously attributed to Au¹⁺ [28,31].

The XPS spectra of the two pre-treated samples were carried out and the obtained spectra concerning Au(4f) are graphically illustrated in Figure 1. Analysis of XPS spectra enables an accurate determination of Au⁰, Au¹⁺, and Au³⁺ present in different pre-treated samples. The computed values of relative abundance of each gold species are given in Table 1. It is clear that Auⁿ⁺/Au⁰ greatly increase with oxygen pre-treatment. An important portion of metallic gold interacted with O₂ yielding trivalent and monovalent gold species. The ratio of the Au and Ce related intensities, I_{Au(4f)}/I_{Ce(3d)}, contains a qualitative information on the Au particle size. Similar values of 0.07±0.01 were obtained (Table 1), indicating similar Au particle sizes after the two pre-treatments. This can be confirmed by the XRD measurements.

3.2. XRD investigation of the pre-treated solids

Figure 2 shows the XRD patterns of oxygen and nitrogen pre-treated samples. The average crystallite size of metallic gold particles was determined, using line broadening profile analysis of the main diffraction peak of the gold (111) by direct application of the Scherrer's equation. The computed values were 7±0.5 nm for both pre-treated catalysts, indicating that the pre-treatment conditions have no effect on the particle size of gold.

3.3. Catalytic properties of different pre-treated solids

Preliminary experiments showed that CeO₂ support material exhibited no measurable catalytic activity at 20-50 °C. Therefore, CeO₂ acts as a catalyst support, while the Au species are the catalytically active constituent in the catalyst under investigation.

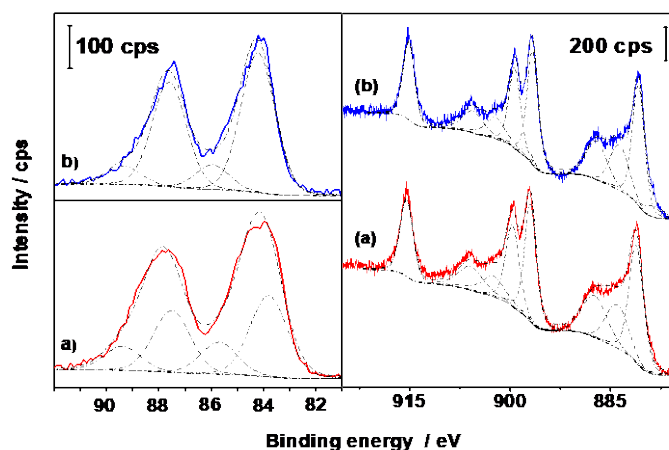


Figure 1. XPS spectra of the Au(4f) region (left panel) and Ce(3d) region (right panel) of different investigated catalysts: (a) Oxygen pre-treated, (b) Nitrogen pre-treated.

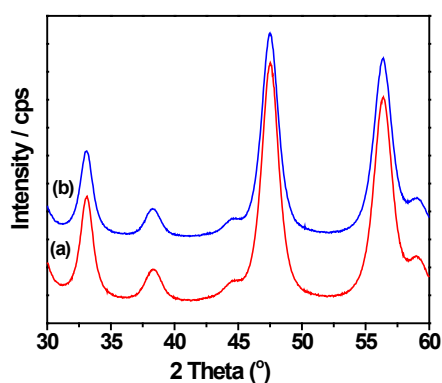


Figure 2. XRD pattern of the Au/CeO₂ catalysts: (a) Oxygen pre-treated, (b) Nitrogen pre-treated.

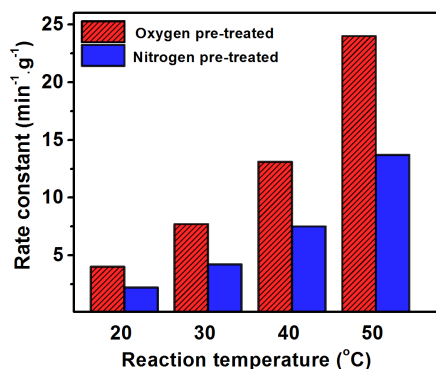


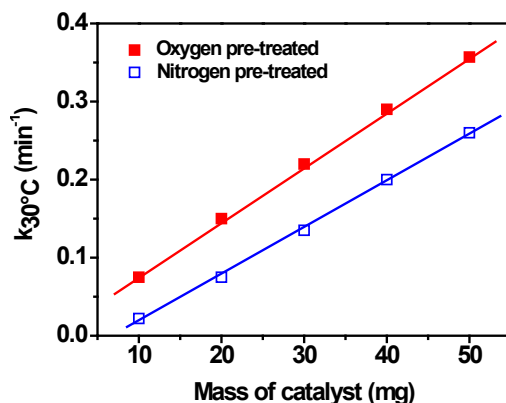
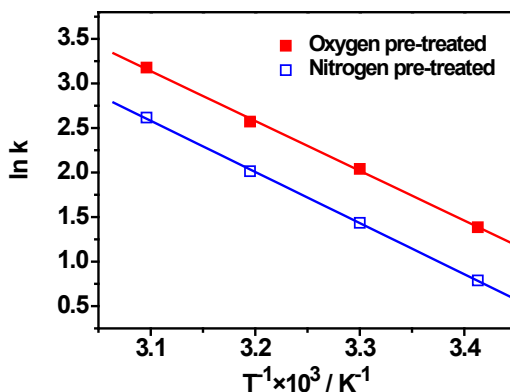
Figure 3. Relationship between the reaction temperature and rate constant for H₂O₂ decomposition over oxygen and nitrogen pre-treated catalyst.

The catalytic reaction was followed by measuring the volume of O₂ gas liberated at different time intervals until no further oxygen evolved. The catalytic reaction was carried out at 20 to 50 °C. First order kinetics (not given) were observed in all cases. The slopes of these plots directly determine the values of a reaction rate constant (k) at a given temperature. Figure 3 shows the relation between the calculated reaction rate constant (k) per gram catalyst and the reaction temperature.

The effect of the mass of catalyst on the rate of decomposition of H₂O₂ was investigated at 30 °C. Figure 4 shows the variation of a reaction rate constant measured at 30 °C ($k_{30^{\circ}\text{C}}$) as a function of mass of oxygen and nitrogen pre-treated catalysts. A good linear relationship was obtained, suggesting the absence of any diffusion phenomenon. So, the mass of the catalyst sample taken for each kinetic experiment varied between 10-50 mg, depending on the catalytic reaction temperature.

Table 2. The values of a first order reaction rate constant measured at different temperatures over oxygen and nitrogen pre-treated Au/CeO₂ catalysts.

Reaction temperature (°C)	Oxygen pre-treated rate constant (min ⁻¹ . g ⁻¹)	Nitrogen pre-treated rate constant (min ⁻¹ . g ⁻¹)
20	4.0	2.2
30	7.7	4.2
40	13.1	7.5
50	24.0	13.7

**Figure 4.** Relationship between the mass of catalyst and rate constant for H₂O₂ decomposition carried out at 30 °C over oxygen and nitrogen pre-treated catalyst.**Figure 5.** Relation between $\ln k$ and $1/T$ for H₂O₂ decomposition carried out over oxygen and nitrogen pre-treated catalyst samples.

The computed values of reaction rate constants (per unit mass) for the reaction carried out at 20 to 50 °C over various catalysts are given in Table 2. The comparison between the activity of oxygen and nitrogen pre-treated solids are better investigated by comparing the k values for reaction carried out at different temperatures.

The computed k values for the oxygen pre-treated sample at any reaction temperatures is about twice the value measured for nitrogen pre-treated sample. As we have shown, the Auⁿ⁺/Au⁰ ratio for oxygen pre-treated sample was about twice for that of nitrogen pre-treated catalyst. So, the Auⁿ⁺ species acted as the most active catalyst's constituent in the investigated system. However, one cannot overlook the role of metallic gold in catalyzing the H₂O₂ decomposition, showing small activity compared to that of cationic gold.

Similar results have been reported for 4.5 wt% Au/CeO₂ using WGS reaction and CO oxidation by oxygen, where the oxygen pre-treated sample showed higher activity than the nitrogen pre-treated one [36-39].

The apparent activation energies (E_a) of H₂O₂ decomposition were determined for both pre-treated samples, from the data of k measured at 20-50 °C. Figure 5 depicts the Arrhenius plot of $\ln k$ as a function of $1/T$ for both catalysts.

The computed E_a values were found to be 46.5 and 47.8 kJ/mol for oxygen pre-treated and nitrogen pre-treated catalysts, respectively. This indicates that the different pre-

treatments of the Au/CeO₂ system do not change the mechanism of the catalyzed reaction, but leads to a change in the concentration of active sites involved in the catalytic reaction. It also supports the assumption that the change in activity between both catalysts referred to the change in Auⁿ⁺ concentration. The standard enthalpies of activation (ΔH^\ddagger) were calculated from the linear plot of the Eyring equation (Figure 6).

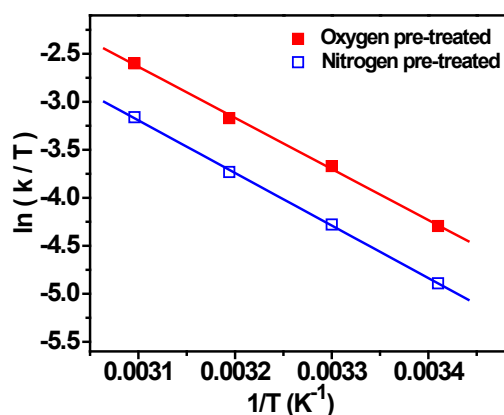
$$\ln\left(\frac{k}{T}\right) = -\frac{\Delta H^\ddagger}{RT} + \ln\left(\frac{k_B}{h}\right) + \frac{\Delta S^\ddagger}{R} \quad (1)$$

where k is the reaction rate constant; T is the absolute reaction temperature; ΔH^\ddagger is the enthalpy of activation; R is the gas constant; k_B is the Boltzmann constant; h is the Planck constant; and ΔS^\ddagger is the standard entropy of activation. The calculated values of activation energies and thermodynamics parameters for activations are given in Table 3.

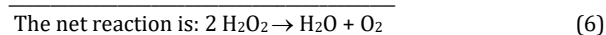
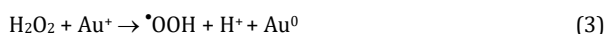
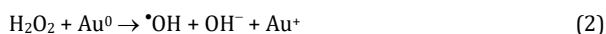
The negative values for ΔS^\ddagger indicate that entropy decreases on forming the activated complex during the catalytic decomposition of H₂O₂ over the given catalyst. It often indicates an associative mechanism in which two reaction partners (hydroxyl (*OH) and hydroperoxyl (*OOH) radicals) form a single activated complex, followed by decomposition to give a final product.

Table 3. Arrhenius activation energies (E_a), standard enthalpies of activation (ΔH^\ddagger), and standard entropy of activation (ΔS^\ddagger) for the decomposition of H_2O_2 over different pre-treated Au/CeO₂ catalysts.

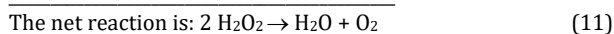
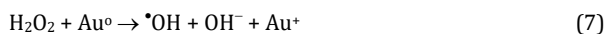
Catalyst pre-treatment	E_a (kJ/mol)	ΔH^\ddagger (kJ/mol)	ΔS^\ddagger (J/mol.K)
Oxygen	46.5	44.3	- 82.2
Nitrogen	47.8	45.5	- 83.0

**Figure 6.** Eyring plots for the determination of the enthalpy and entropy of activation for the catalytic decomposition of H_2O_2 over different pre-treated Au/CeO₂ catalysts.

The proposed mechanisms for the catalytic decomposition of H_2O_2 into hydroxyl and hydroperoxyl radicals in the presence of nanosized Au/CeO₂ by a redox cycle [40], can be discussed as follows:

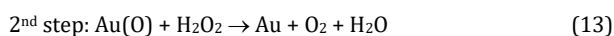
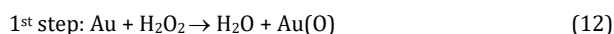


Another suggested mechanism can be interpreted as follows [41];



He *et al.* [7] demonstrated that Au nanoparticles exhibited intrinsic catalytic activity, resulting in the generation of hydroxyl radicals and oxygen as well as scavenging superoxide. In the presence of H_2O_2 , Au nanoparticles (NPs) can elicit the generation of hydroxyl radicals in an acidic environment and the production of oxygen under alkaline conditions.

A third suggested mechanism can be illustrated as follows [42];



where Au(O) is the chemisorbed oxygen onto gold catalyst.

Comparing the obtained results with those previously reported for CuO/CeO₂ system containing 8.5 wt% CuO [4,5], it is clear that the activity of Au/CeO₂ catalyst in H_2O_2 decomposition carried out at 30 °C is 8-fold greater than that measured for CuO/CeO₂ system.

4. Conclusions

Nanosized Au/CeO₂ catalyst containing 4.5 wt% gold prepared by deposition-precipitation procedure, shows an excellent catalytic activity towards H_2O_2 decomposition. The calculated crystallites size of the gold particles is 7.0 ± 0.5 nm for oxygen and nitrogen pre-treated samples. Heating at oxidative atmosphere had a great impact on the presence of cationic gold (Au^{n+}) as determined by (XPS). The Au^{n+}/Au^0 ratio was much higher in oxygen pre-treated sample than that of nitrogen pre-treated sample. The catalytic activity of oxygen pre-treated sample was about twice higher than that measured for nitrogen pre-treated one. This finding ran parallel to the extent of Au^{n+} present in the oxygen and nitrogen pre-treated catalysts.

Acknowledgements

I am grateful to Institute of Surface Chemistry and Catalysis, Ulm University, Germany, for XPS measurements.

ORCID

Ayman Abd El-Moemen

 <http://orcid.org/0000-0001-7037-6490>

References

- [1]. Lousada, C. M.; Jonsson, M. *J. Phys. Chem.* **2010**, *114*, 11202- 11208.
- [2]. Lousada, C. M.; Johansson, A. J.; Brinck, T.; Jonsson, M. *J. Phys. Chem. C* **2012**, *116*, 9533-9543
- [3]. Naya, S.; Teranishi, M.; Kimura, K.; Tada, H. *Chem. Commun.* , **2011**, *47*, 3230-3232.
- [4]. El-Shobaky, G. A.; Radwan, F. M.; Turky, A. M.; Abd El-Moemen, A. *Adsorp. Sci. Technol.* **2000**, *18*, 799-811.
- [5]. El-Shobaky, G. A.; Radwan, F. M.; Turky, A. M.; Abd El-Moemen, A. *Adsorp. Sci. Technol.* **2001**, *19*, 779-793.
- [6]. Moreno, T.; Garcia-Serna, J.; Jose Cocero, M. *J. Supercrit. Fluids* **2011**, *57*, 227-235.

- [7]. He, W.; Zhou, Y. T.; Wamer, W. G.; Hu, X.; Wu, X.; Zheng, Z.; Boudreau, M. D. Yin, J. J. *Biomaterials* **2013**, *34*, 765-773.
- [8]. Khetre, S. M.; Jadhav, H. V.; Bangale, S. V.; Jagdale, P. N.; Bamane, S. R. *Adv. Appl. Sci. Res.* **2011**, *2*, 252-259.
- [9]. Ghozza, A. M. *Matter Lett.* **2003**, *57*, 2120-2129.
- [10]. Zhou, H.; Shen, Y. F.; Wang, J. Y.; Chen, X.; O'Young, C. L.; Suib, S. L. *J. Catal.* **1998**, *176*, 321-328.
- [11]. Dantas, T. L. P.; Mendonca, V. P.; Jose, H. J.; Rodrigues, A. E.; Moreira, R. *Chem. Eng. J.* **2006**, *118*, 77-82.
- [12]. Cuzzola, A.; Bernini, M.; Salvadori, P. *Appl. Catal. B.* **2002**, *36*, 231-237.
- [13]. Moura, F. C. C.; Oliveira, G. C.; Araujo, M. H.; Ardisson, J. D.; Macedo, W.; Lago, R. M. *Appl. Catal. A.* **2006**, *307*, 195-204.
- [14]. Vielstich, W.; Gasteiger, H. A.; Lamm, A., *Fuel Cell Technology and Applications Part I*. John Wiley & Sons, New York, 2003, pp. 648-662.
- [15]. Trimm S. D. L.; Onsan, Z. I. *Catal. Rev.* **2001**, *43*, 31-84.
- [16]. Sethuraman, V. A.; Weidner, J. W.; Haug, A. T.; Motupally, S.; Protsailo, L. V. *J. Electrochem. Soc.* **2008**, *155(1)*, 50-57.
- [17]. Burch, R. *Phys. Chem. Chem. Phys.* **2006**, *8*, 5483-5500.
- [18]. Andreeva, D.; Ivanov, I.; Ilieva, L.; Sobczak, J. W.; Avdeev, G.; Petrov, K. *Top. Catal.*, **2007**, *44*, 173-182.
- [19]. Fu, Q.; Weber, A.; Flytzani-Stephanopoulos, M. *Catal. Lett.* **2001**, *77*, 87-95.
- [20]. Fu, Q.; Kudriavtseva, S.; Saltsburg, H.; Flytzani-Stephanopoulos, M. *Chem. Engin. J.* **2003**, *93*, 41-53.
- [21]. Haruta, M.; Yamada, N.; Kobayashi, T.; Iijima, S. *J. Catal.* **1989**, *115*, 301-309.
- [22]. Bond, G. C.; Thompson, D. T. *Catal. Rev. Sci. Eng.* **1999**, *41*, 319-388.
- [23]. Concepcion, P.; Carrettin, S.; Corma, A. *Appl. Catal. A.* **2006**, *307*, 42-45.
- [24]. Han, Y. F.; Phonthammachai, N.; Ramesh, K.; Zhong, Z.; White, T. *Environ. Sci. Technol.* **2008**, *42*, 908-912.
- [25]. Kiyonaga, T.; Jin, Q.; Kobayashi, H.; Tada, H. *Chem. Phys. Chem.* **2009**, *10*, 2935-2938.
- [26]. Luo, T.; Vohs, J. M.; Gorte, R. J. *J. Catal.* **2002**, *210*, 397-404.
- [27]. Fu, Q.; Saltsburg, H.; Flytzani-Stephanopoulos, M. *Science* **2003**, *301*, 935-938.
- [28]. Kim, C. H.; Thompson, L. T. *J. Catal.* **2006**, *244*, 248-250.
- [29]. Karpenko, A.; Leppelt, R.; Plzak, V.; Behm, R. J. *J. Catal.* **2007**, *252*, 231-242.
- [30]. Deren, J.; Haber, J. *J. Catal.* **1965**, *4*, 22-33.
- [31]. Fu, Q.; Deng, W.; Saltsburg, H.; Flytzani-Stephanopoulos, M. *Appl. Catal. B* **2005**, *56*, 57-68.
- [32]. Holm, R.; Storp, S. *Appl. Phys.* **1976**, *9*, 217-222.
- [33]. Pireaux, J. J.; Liehr, M.; Thiry, P. A.; Delrue, J. P.; Caudano, R. *Surf. Sci.* **1984**, *141*, 221-232.
- [34]. Briggs, D.; Seah, M. P. *Practical Surface Analysis-Auger and X-Ray Photoelectron Spectroscopy*. John Wiley & Sons, Chichester, 1990.
- [35]. Moulder, J. F.; Stickle, W. F.; Sobol, P. E.; Bomben, K. D. *Handbook of X-ray Photoelectron Spectroscopy*, Perkin Elmer Corp., Eden Prairie, USA, 1992.
- [36]. Abd El-Moemen, A.; Karpenko, A.; Denkwitz, Y.; Behm, R. J. *J. Power Sources* **2009**, *190*, 64-75.
- [37]. Abd El-Moemen, A.; Kucerova, G.; Behm, R. J. *Appl. Catal. B* **2010**, *95*, 57-70.
- [38]. Abd El-Moemen, A.; Abdel-Mageed, A. M.; Bansmann, J.; Parlinska-Wojtan, M.; Behm, R. J.; Kucerova, G. *J. Catal.* **2016**, *341*, 160-179.
- [39]. Bansmann, J.; Kucerova, G.; Abdel-Mageed, A. M.; Abd El-Moemen, A.; Behm, R. J. *J. Electr. Spectrosc. Relat. Phenom.* **2017**, *220*, 86-90.
- [40]. Dominguez, C. M.; Quintanilla, A.; Casas, J. A.; Rodriguez, J. J. *Chem. Eng. J.* **2014**, *253*, 486-492.
- [41]. Rezwani, M. M.; Ohsaka, T. *Anal. Chem.* **2006**, *78*, 1200-1205.
- [42]. Serra-Maia, R.; Bellier, M.; Chastka, S.; Tranhuu, K.; Subowo, A.; Rimstidt, J. D.; Usov, P. M.; Morris, A. J.; Michel F. M. *ACS Appl. Mater. Interfaces* **2018**, *10(25)*, 21224-21234.



Copyright © 2019 by Authors. This work is published and licensed by Atlanta Publishing House LLC, Atlanta, GA, USA. The full terms of this license are available at <http://www.eurjchem.com/index.php/eurjchem/pages/view/terms> and incorporate the Creative Commons Attribution-Non Commercial (CC BY NC) (International, v4.0) License (<http://creativecommons.org/licenses/by-nc/4.0>). By accessing the work, you hereby accept the Terms. This is an open access article distributed under the terms and conditions of the CC BY NC License, which permits unrestricted non-commercial use, distribution, and reproduction in any medium, provided the original work is properly cited without any further permission from Atlanta Publishing House LLC (European Journal of Chemistry). No use, distribution or reproduction is permitted which does not comply with these terms. Permissions for commercial use of this work beyond the scope of the License (<http://www.eurjchem.com/index.php/eurjchem/pages/view/terms>) are administered by Atlanta Publishing House LLC (European Journal of Chemistry).